Loss Function Modeling of Efficiency Maps of Electrical Machines

# Loss Function Modeling of Efficiency Maps of Electrical Machines

Amin Mahmoudi, Wen L. Soong
School of Electrical and Electronic Engineering
University of Adelaide, Australia
amaminmahmoudi@gmail.com
wen.soong@adelaide.edu.au

Gianmario Pellegrino, Eric Armando
Politecnico di Torino, Corso Duca degli Abruzzi 24, Torino, 10129 Italy
gianmario.pellegrino@polito.it
eric.armando@polito.it

***Abstract*— This paper presents a novel approach in modeling of efficiency maps for electrical machines. It is based on sum of the terms in the form of $k_{mn}T^m\omega^n$ to represent the variation of the stator and rotor copper, iron and magnet losses with torque and speed. The effect of each term on the shape of the efficiency map is explored. Analysis is performed on the calculated efficiency and loss maps of an induction, an interior permanent magnet and a surface permanent magnet machine to demonstrate the validity of the approach.**

**Keywords— efficiency map, electric machines, induction machines, loss modeling, permanent magnet machines**

## I. INTRODUCTION

### A. Background

An efficiency map for an electrical machine is a contour plot of the maximum efficiency on the torque (or power) – speed plane. Its envelope shows the maximum torque capability of the machine as a function of speed.

Efficiency maps are widely used for describing the performance of electric motors and drives as a function of their torque/speed operating points. For vehicle propulsion drives, energy usage over standard driving cycles and hence an expected driving range can be determined via manipulation of the efficiency map of the electrical machine [1,2]. To minimize energy usage, the efficiency should be maximum in the operating regions where the machine has the highest average output power over the driving cycle.

Permanent magnet (PM) machines are widely used for traction applications due to their high power density, and their ability to be designed for a wide flux-weakening range. Conventionally, the two main control parameters are the *d*- and *q*-axis currents $I_d$ and $I_q$. Two main constraints are the input voltage and current limits of machine. The induction motor (IM) has also been applied in electric traction, with commercial success [3].

Efficiency maps are obtained by finding the maximum efficiency for a given speed and torque by examining the combinations of control parameters, such as $I_d$ and $I_q$ for PM machines, which give the desired torque and finding a combination with highest efficiency within the voltage and current limits. This is done using analytical, finite-element or experimental techniques. A similar approach based on $I_d$ and $I_q$ for induction machines has recently been described [4].

While the process of generating and using efficiency maps of electrical machines is well-known [1-2,5-9], there has been little research on the interpretation and analysis of efficiency maps, as well as on loss modelling of the machine as a whole, as a function of torque and speed, rather than modelling of local loss phenomena. Presently comparisons between measured and calculated efficiency maps have been largely limited to showing contour plots of the difference between them [8].

This paper examines use of the loss function modeling techniques to understand how different loss types affect the shape of an efficiency map and how experimental efficiency and loss maps can be analysed and also compared with simulation results.

### B. Loss Function Modeling of Efficiency Maps

The key novel contribution of this work is to model the power losses of the electrical machine at a given torque $T$ and speed $\omega$ as the sum of loss terms of the form $T^m\omega^n$ where $m$ and $n$ are integers [10].

Heins et al. [11] have previously done loss component modelling for electrical machines using loss terms which are a function of current $I$ and speed $\omega$, that is $I^m\omega^n$, rather than torque $T$ and speed $\omega$, see Table I. Their emphasis was on modelling the breakdown of losses in the machine and comparing finite-element (FE) and experimental results. Their discussion was limited to only permanent magnet machines and did not examine efficiency maps.

Normally when comparing FE and test results, the total FE loss is compared with the measured loss for different operating points. The novelty of Heins' contribution is to compare the loss component functions instead of the loss values at each operating point. This is shown in Table I where the sum of the calculated loss function coefficients for each type of loss is compared with the measured data. This comparison provides more information about the likely types of losses which are responsible for the discrepancy between the experimental and measured results. For instance in Table I, the loss term with the largest error is loss $\propto \omega$ which is produced by the mechanical and core losses.

TABLE I. COMPARISON OF FE AND EXPERIMENTAL CURRENT-SPEED LOSS COMPONENTS [11]

| | | 1 | | | $i^2$ | | |
|---|---|---|---|---|---|---|---|
| | | $\omega$ | $\omega^2$ | $\omega^3$ | 1 | $\omega$ | $\omega^2$ |
| FEA | Core Loss (W) | 23 | 9 | 0 | 0 | 5 | 1 |
| | Solid Loss (W) | 0 | 0 | 0 | 0 | 4 | 1 |
| | Copper (W) | 0 | 0 | 0 | 52 | 0 | 2 |
| | Mechanical (W) | 30 | 0 | 0 | 0 | 0 | 0 |
| | Total (W) | **53** | **9** | **0** | **52** | **9** | **4** |
| Experimental | | **93** | **10** | **0** | **60** | **18** | **0** |
| Difference | | **40** | **1** | **0** | **8** | **9** | **-4** |

In this paper, the loss maps of three traction machines are modelled, and the corresponding efficiency maps are analysed. The key changes from Heins' work are firstly that torque is used in place of current as the metric of the machine's load. Secondly, magnetic saturation not previously considered is here taken into account. Thirdly, this study also includes induction machines while the previous study was limited to permanent magnet machines. Finally this work includes field-weakening operation and not only constant torque operation as done previously.

The results of this work are based on finite-element analysis. One induction machine, one interior PM and one surface PM machine are considered as test cases. A similar approach to that shown in Table I is used: for each machine, each of the calculated loss types (e.g. stator copper loss) is modeled as a sum of loss functions. While experimental results of three such machines designed for the same vehicle specifications are not available, the calculated loss maps are analysed instead. This FEA approach is still considered valid because the literature shows that FEA evaluated loss maps match experimental loss maps with good accuracy [8].

The paper is organized as follows: a discussion of the electrical machine analytical modelling under constant torque and constant power operation is presented in Section II. Section III then describes the finite-element based calculation of efficiency/loss maps for the three machines and shows the detailed loss modeling results. Section IV examines the process of loss function modeling. Section V gives a detailed discussion of the results and Section VI examines some aspects of the interpretation of efficiency maps.

## II. LOSS FUNCTIONS PRINCIPLE AND CONCEPTS

### A. PM Machine Example

It is proposed that the power loss $P_{loss}$ in an electrical machine under maximum efficiency operation can be expressed as a function of torque $T$ and speed $\omega$ in the form,

$$P_{loss}(T,\omega) \approx \sum k_{mn} T^m \omega^n \qquad (1)$$

where the exponents $m$ and $n$ are integers, and the constants $k_{mn}$ are non-negative. Thus the efficiency is given in terms of output power $P_o$ as,

$$\eta(T,\omega) = \frac{P_o}{P_{loss}(T,\omega) + P_o} = \frac{T\omega}{P_{loss}(T,\omega) + T\omega} \qquad (2)$$

Equation (2) can also be used to find the loss map $P_{loss}(T,\omega)$ given the efficiency map $\eta(T,\omega)$.

For example, consider a simple loss model for a surface PM machine. The iron loss is assumed proportional to $\omega^2$ which only considers eddy-current loss and neglects armature reaction (stator current) effects. The torque is assumed proportional to current (neglecting saturation and assuming a constant current angle) and hence the stator copper loss is proportional to $T^2$. Thus to a first approximation the surface PM machine loss can be described as,

$$P_{loss}(T,\omega) = k_{20} T^2 + k_{02} \omega^2 \qquad (3)$$

This is illustrated in Fig. 1 which shows the copper, iron and total loss terms as well as the efficiency map as contour plots with torque and speed axes.

The copper loss plot, Fig. 1(a), is only a function of torque and so consists of horizontal contours while the iron loss, Fig. 1(b), is only a function of speed and consists of vertical contours. The spacing of these contours is non-uniform due to the square law dependance. The total loss plot, Fig. 1(c), being the sum of a torque squared and a speed squared component has elliptical contours centred on the origin. The resultant efficiency map, Fig. 1(d), shows linear contours passing through the origin with maximum efficiency when the torque and speed are roughly equal in magnitude.

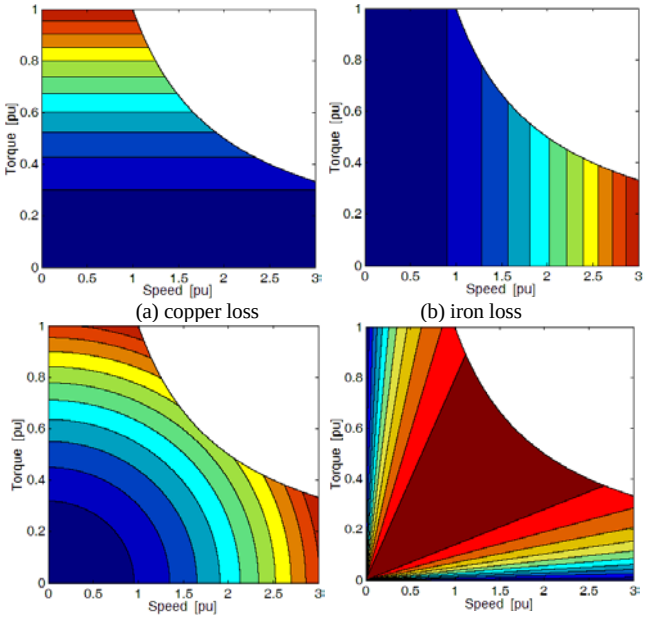


Figure 1. Example surface PM machine results as contour plots on axes of torque and speed, (a) copper loss, (b) iron loss, (c) total loss, (d) efficiency.

The proposed analysis in this paper is to convert an efficiency map as shown in Fig. 1(d), to an equivalent loss map in Fig. 1(c) and then curve fitting this as loss terms of the form $T^m\omega^n$, Fig. 1(a) and (b).

### B. *Loss and Efficiency Plots for $T^m\omega^n$ Terms*

Fig. 2(a) shows a 4-by-4 matrix of contour plots representing examples of power loss components of the form $k_{mn}T^m\omega^n$, as a function of torque and speed. The lower left plot refers to $k_{00}T^0\omega^0$, representing a constant loss component (independent of torque and speed). The plots in the left-most

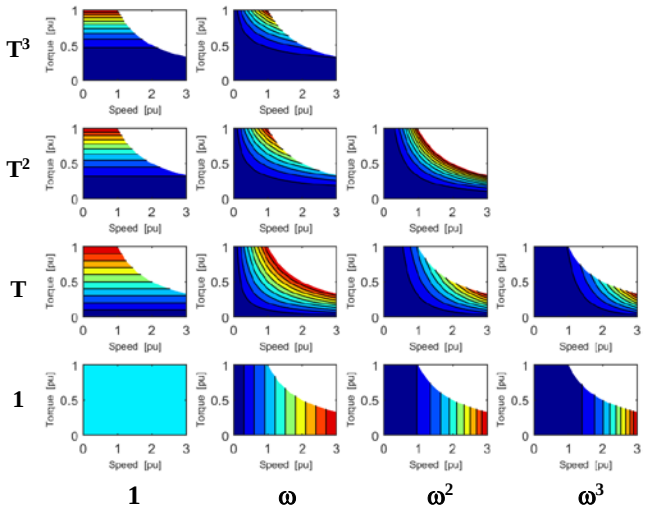


(a) power loss contours in form $T^m\omega^n$

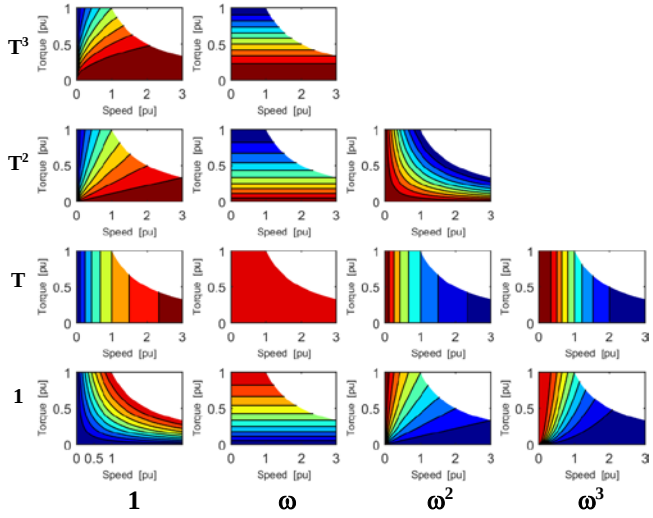


(b) efficiency contours

Figure 2. Contour plots of (a) power loss and (b) efficiency on axes of torque versus speed for loss terms of the form $k_{mn}T^m\omega^n$ where $m + n \le 4$ [10]

column represent terms related to only torque (1, $T$, $T^2$ and $T^3$). Finally, the bottom row represents terms related to only speed (1, $\omega$, $\omega^2$, $\omega^3$). In each of the loss terms, the lowest loss occurs at the origin, for zero torque and speed. The higher the order of the considered loss term (that is, the greater the value of $m + n$), the more steeply the loss increases. The figure includes the $T^2$ and $\omega^2$ terms from Figs. 1(a) and (b). Only terms where $m + n \le 4$ are shown (not including $T^4$ and $\omega^4$).

Fig. 2(b) shows the shape of the efficiency plots, obtained from (2), corresponding to each loss term in Fig. 2(a).

The relationship between each loss term $T^m\omega^n$ and the resultant efficiency map is given by,

$$\eta\left(T^m,\omega^n\right)=\frac{T\omega}{T\omega+T^m\omega^n}=\frac{1}{1+T^{m-1}\omega^{n-1}}\approx 1-T^{m-1}\omega^{n-1} \quad (4)$$

The simplification in (4) holds for small values of $T^{m-1}\omega^{n-1}$. Thus, the shape of the efficiency plots is similar (but opposite in "slope") to that of the loss plots one row down and one column left. The natural "centre" of the matrix of efficiency plots is the one corresponding to the loss term $k_{11}T\omega$, which has a constant value of efficiency at all operating points. For all the other efficiency maps in the matrix, the highest efficiency (red shading) is the point or line closest to this "centre" plot in the matrix. Thus for the constant loss term $k_{00}T^0\omega^0$, the efficiency increases with the product of torque and speed while for the loss term $k_{22}T^2\omega^2$, the efficiency decreases with the product of torque and speed. In addition, the further a given plot is from the "centre" plot, the steeper the efficiency gradient within that plot.

A practical machine has multiple sources of loss, each of which influences the shape of its efficiency map. For instance in the surface PM machine example in Fig. 1, the total efficiency map is a combination of the efficiency maps for the $T^2$ and $\omega^2$ terms. Thus by analysis of an efficency map, it is also possible to determine the key loss terms.

### C. *Prediction of Key Loss Terms*

The simplified machine analysis presented in this sub-section is applicable to induction machines (IM) as well as to surface PM (SPM) and interior PM (IPM) machines. Such analysis will be used to determine the likely key loss function terms for each machine, both in the constant-torque and constant-power operating regions.

The stator copper loss is proportional to the square of the stator current.

Consider the copper losses in the constant torque region. For SPM machines, $T \propto I$ and thus the copper loss $\propto T^2$. For the IM and for IPMs with a low value of magnet flux, at low currents the torque $\propto I^2$ and thus copper loss $\propto T$, however at moderate currents saturation causes the torque $\propto I$ and hence copper loss $\propto T^2$. Thus both $T$ and $T^2$ loss terms would be expected. Some machines saturate heavily at high currents. For instance if due to heavy saturation $T \propto \sqrt{I}$ then this would result in a copper loss $\propto T^4$.

Consider the copper losses in the constant power region. For IMs or IPMs with a low value of magnet flux, we can assume a constant voltage and a relatively constant power-factor, then the current should be proportional to output power ($\propto T\omega$), thus the copper loss $\propto T^2\omega^2$. For SPM (and IPM machines with a high values of magnet flux), due to the large $d$-axis field-weakening current component the stator current is more influenced by speed than torque, hence the

largest copper loss terms should have $m < n$, e.g. terms such as $T\omega^2$, $T\omega^3$, $\omega$, $\omega^2$, or $\omega^3$.

The iron loss consists of hysteresis and eddy-current terms which are a function of the flux density $B$ and the frequency (and hence speed $\omega$). To a first approximation, hysteresis loss $\propto B^2\omega$ and eddy-current loss $\propto B^2\omega^2$.

Consider the constant torque region. The magnet flux density is constant and independent of torque $T$ and hence produces iron loss terms $\omega$ and $\omega^2$. The flux density from the stator current is largely proportional to torque and thus the iron loss from the stator current is related to torque squared resulting in $T^2\omega$ and $T^2\omega^2$ terms.

In the (high speed) constant power region, the eddy-current loss normally dominates and the fundamental flux in the machine falls inversely with speed. Thus the fundamental iron loss should not depend on speed. The IM torque should be roughly proportional to flux squared, thus the fundamental iron loss should be proportional to torque. IPM machines under field-weakening conditions can have high harmonic loss components which increase rapidly with speed. In [13] under short-circuit conditions (constant $I_d$), the (harmonic) iron loss increased with the square of speed.

The magnet losses are due to eddy-currents in the conductive magnets and consist of stator slotting effects ($\omega^2$) and armature reaction components ($T^2\omega^2$). These can be significant in SPM machines where the magnets are exposed to the airgap flux but are usually small in IPM machines due to the buried magnets.

Mechanical losses include bearing (typically modelled as a constant loss torque, hence $\omega$), and windage losses, typically modelled as $\omega^2$ or $\omega^3$ terms [11].

Using the above modelling approach, the expected key loss terms of the form $k_{mn}T^m\omega^n$ can be identified. These are summarized in Table II. Both the constant torque and constant power regions are examined for each machine. The following terms are used in the table: copper losses in the stator and rotor (cu), iron loss (fe), magnet losses (mg) and windage losses (wdge). From the analysis, the main loss components appear to occur with $m + n \leq 4$. As indicated at the start of this subsection, heavy saturation can cause loss terms of the form copper loss $\propto T^4$ which are not shown in Table II.

It is to be noted that loss terms similar to those of terms in Table II are expected for other motor types. The type of loss terms are not expected to be sensitive to the size of the motor though clearly the relative contribution of each loss does vary with motor size.

TABLE II. PREDICTED LOSS TERMS CORRESPONDING TO DIFFERENT LOSS MECHANISMS [10]

| **Induction Machine** | | | | | | | | |
|---|---|---|---|---|---|---|---|---|
| | **Constant Torque** | | | | **Constant Power** | | | |
| $\mathbf{T^3}$ | | | | | | | | |
| $\mathbf{T^2}$ | cu | fe | fe | | | | cu | |
| **T** | cu | | | | fe | | | |
| **1** | | fe/brg | fe | wdge | | brg | | wdge |
| | **1** | $\boldsymbol{\omega}$ | $\boldsymbol{\omega^2}$ | $\boldsymbol{\omega^3}$ | **1** | $\boldsymbol{\omega}$ | $\boldsymbol{\omega^2}$ | $\boldsymbol{\omega^3}$ |

| **Interior PM Machine** | | | | | | | | |
|---|---|---|---|---|---|---|---|---|
| | **Constant Torque** | | | | **Constant Power** | | | |
| $\mathbf{T^3}$ | | | | | | | | |
| $\mathbf{T^2}$ | cu | fe | fe | | | | cu/fe | |
| **T** | cu | | | | | | | |
| **1** | | fe/brg | fe | wdge | | brg | fe | wdge |
| | **1** | $\boldsymbol{\omega}$ | $\boldsymbol{\omega^2}$ | $\boldsymbol{\omega^3}$ | **1** | $\boldsymbol{\omega}$ | $\boldsymbol{\omega^2}$ | $\boldsymbol{\omega^3}$ |

| **Surface PM Machine** | | | | | | | | |
|---|---|---|---|---|---|---|---|---|
| | **Constant Torque** | | | | **Constant Power** | | | |
| $\mathbf{T^3}$ | | | | | | | | |
| $\mathbf{T^2}$ | cu | fe | fe/mg | | | | mg | |
| **T** | | | | | | | cu | cu |
| **1** | | fe/brg | fe/mg | wdge | | fe/brg/ cu | fe/mg/ cu | cu/ wdge |
| | **1** | $\boldsymbol{\omega}$ | $\boldsymbol{\omega^2}$ | $\boldsymbol{\omega^3}$ | **1** | $\boldsymbol{\omega}$ | $\boldsymbol{\omega^2}$ | $\boldsymbol{\omega^3}$ |

## III. FINITE-ELEMENT CALCULATION OF EFFICIENCY MAPS

### *A. Three Example 50-kW, 12-kr/min Machine Designs*

Three example machines designed for a traction application are compared. An induction motor (IM), interior permanent magnet motor (IPM) and surface permanent magnet (SPM) motor design for the same 50-kW, 12-kr/min electric traction application were considered [10,14-15]. Their cross-sections are shown in Fig. 3. All the machines have the same stack length and stator outer diameter. The key parameters of the motors are reported in Table III.

Finite-element analysis was used to predict their performance characteristics [15], including the maximum torque versus speed capability envelope and the contour plots of the minimum loss and maximum efficiency.


Figure 3. Cross-sections of the three machines [15]

TABLE III. SPECIFICATIONS OF THREE 50-KW, 12 KR/MIN MOTORS

| | IM | IPM | SPM |
|---|---|---|---|
| **Key Dimensions** | | | |
| - stator outer diameter | | 216 mm | |
| - airgap length | | 0.7 mm | |
| - stack length | | 170 mm | |
| **Design Parameters** | | | |
| - poles | 4 | 4 | 4 |
| - stator slots | 48 | 48 | 6 |
| - slots per pole per phase (SPP) | 4 | 4 | 0.5 |
| - copper slot fill (copper/slot area) | 40% | 40% | 40% |
| **Mechanical Parameters** | | | |
| - continuous torque at 3.2 kW loss | 110 Nm | 160 Nm | 130 Nm |
| - rated speed at continuous torque | 4.0 kr/min | 3.8 kr/min | 3.8 kr/min |
| - overload torque capability | 210 Nm | 210 Nm | 150 Nm |
| **Electrical Parameters** | | | |
| - rated voltage (rms line) | 212 V | 212 V | 212 V |
| - back-emf at 12 krpm (20°C) | - | 0.98 pu | 3.12 pu |
| - characteristic current (rms 150°C) | - | 145 A | 136 A |
| - stator resistance (150°C) | 27mΩ | 27mΩ | 21mΩ |
| **Magnets** | | | |
| - type | - | NdFeB | NdFeB |
| - remanent flux density | - | 1.26 T | 1.26 T |

### *B. Finite-Element Loss Map Evaluation*

For the machines the performance characteristics were calculated at a fixed speed (3,500 r/min), using the Magnet/Infolytica 2D finite-element package [16] over the expected $I_d$, $I_q$ operating range of each machine. The calculated characteristics are the torque, stator flux-linkage and losses.

The losses include the iron losses (stator and rotor eddy-current and hysteresis losses) and the PM eddy-current loss. Harmonic fields and rotational excitation effects are taken into account in the iron loss calculations [16]. The loss results can be scaled to any desired speed using the appropriate co-efficient for the hysteresis loss (1.231 for the steel used) and a square-law term for the eddy-current losses [17]. The calculated PM loss from the 2D analysis was reduced by 40% to take into account the magnet dimensions [18].

For the IM machine, the analysis procedure described in [4] was used. The steady-state rotor bar currents corresponding to the stator $I_d$ and $I_q$ currents were found using a three-step static FEA procedure. The rotor loss was then found using the rotor geometry and an estimated rotor temperature (180°C).

The above results allow the calculation of the minimum losses and hence maximum efficiency for a given torque and speed while meeting the system voltage (212Vrms line) and current constraints (255 Arms). This allows the calculation of the torque-speed contour plots of efficiency, total loss and each of the loss contributions shown in Fig. 4.

The FE calculated loss contour plots in Fig. 4 were curve-fitted using terms of the order of $T^m\omega^n$. The corresponding tabulated co-efficients for each curve fit are shown in Fig. 5. The loss contour plots corresponding to these tabulated fitted co-efficients are shown in Fig. 4 to give an indication of the accuracy of the curve fit for each loss type.

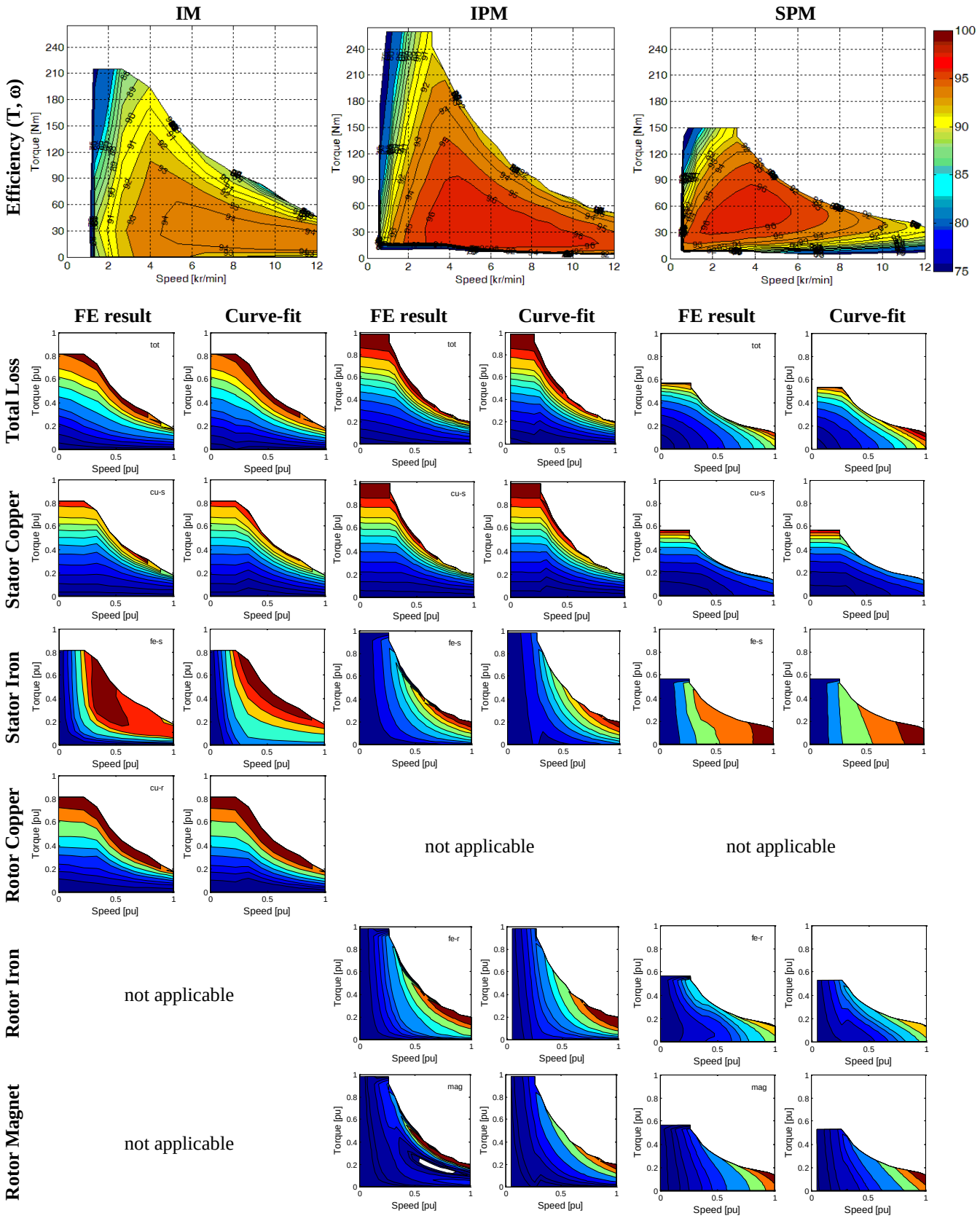


Figure 4. The FE calculated efficiency maps [10] and loss contours for the IM, IPM and SPM machines. For the loss contours the calculated result is on the left and the curve-fitted result is on the right.

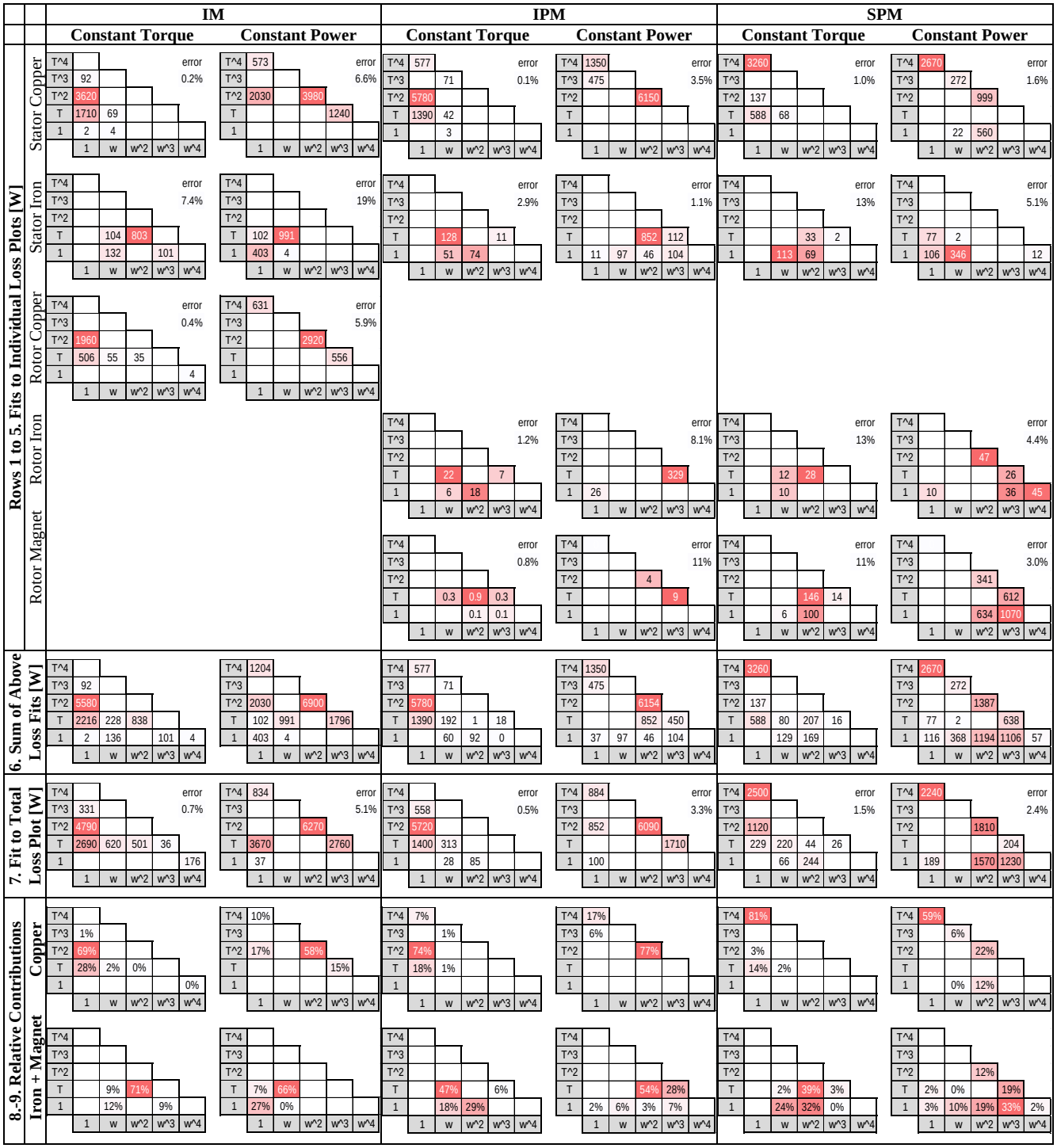


Figure 5. The curve fit results corresponding to the loss contour plots in Fig. 4 for the constant torque and constant power regions for each machine and loss type. It considers loss co-efficients up to $m + n \leq 4$. Rows 1 to 5 are the curve fits for the five individual loss types where the peak loss co-efficients are given in watts. Row 6 is the sum of the co-efficients for the above five loss fits. Row 7 is the curve fit for the total loss contour plot. Row 8 is the sum of the co-efficients for the stator and rotor copper losses and Row 9 is the sum of the co-efficients for the non-copper losses. For these last two rows, within each matrix, the loss terms are normalised to a total of 100% to show the distribution of losses between the co-efficients.

## IV. Curve-Fitting Using Loss Functions

This section discusses the curve-fitting of the FE calculated loss contour plots in Fig. 4 using loss functions. It covers three aspects: the selection of the degree (the maximum value of $m + n$) of the co-efficients; the effect of allowing negative loss co-efficients; and the effect of not partitioning the loss contours into a constant torque and constant power regions.

Equation (1) is normalised to simplify the curve fitting process,

$$P_{loss}(T,\omega) = \sum k_{mn} \left(\frac{T}{T_b}\right)^m \left(\frac{\omega}{\omega_b}\right)^n \quad \text{pu} \qquad (5)$$

where for the machines considered, the base torque $T_b$ is 265 Nm, the base speed $\omega_b$ is 12 kr/min and the base power of the losses is 8 kW, which is the approximate maximum loss of the IPM machine.

The IPM efficiency and loss values were calculated using finite-element analysis at 20 speeds for 16 torque values giving a total of 320 points, as shown in Fig. 6. These are partitioned into the constant torque region (6 speed values) and the constant power region (11 speed values). These regions overlap one another by one speed value.

The SPM has the same number of data points, while the IM has one-quarter of the number of data points. Thus for the IM there were 8 torque values at 10 speeds giving 80 points which were partititioned into 3 speed values for the constant torque region and 8 speed values for the constant power region.

The number of values in each axis should therefore be sufficient for a 4th order polynomial, except for speed points of the IM in the constant torque region.

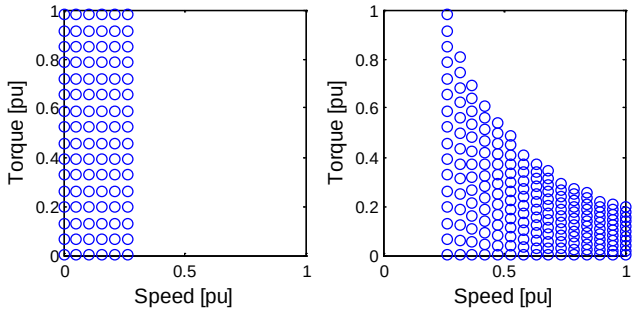


Figure 6. IPM loss and efficiency contour plot calculated data points, constant torque region (left) and constant power region (right).

### A. Effect of Order of Co-efficients

The IPM stator copper loss contour plot is shown in Fig. 4 (3rd row, 3rd column). The co-efficients resulting from modeling this using non-negative loss terms of maximum degree $m+n$ from 0 to 5 are shown in Fig. 7, for the constant torque and constant power regions. The values of the co-efficients shown are the maximum loss contribution of each term in watts over the corresponding region of interest. Shading is used to show the relative magnitudes of the terms within each set of co-efficients. The rms modelling error of all the FE calculated points in the region of interest is indicated on the right as a percentage of the peak calculated value of the loss in that region.

The co-efficients were obtained using the Matlab curve-fitting toolbox (cftool v3.2.1) [19] for a polynomial fit of the appropriate degree for the normalised quantities, see (5). A constraint was set that all co-efficients not be negative.

In Fig. 7 the zero-degree model is simply a constant loss which results in a large modelling error of 20 to 30%. This is improved by considering higher degree models. The 1st degree model includes the additional terms $T$ and $\omega$ which reduces the error to 10 to 12%. The 2nd degree model includes the additional loss terms $T^2$, $T\omega$ and $\omega^2$. Finally the 5th degree model includes terms of $T^5$, $T^4\omega$, ... $\omega^5$.

By observing the reduction in modeling error with the increase in the maximum degree used, it is seen that for the stator copper loss of the IPM machine, a 3rd degree equation is suitable for the constant torque region and a 4th degree equation is required for the constant power region. It can also be seen that once the degree increases beyond a certain point some loss co-efficients are fairly stable in magnitude indicating they are "true" loss terms, e.g. the $T$ and $T^2$ terms in the constant torque region, while others appear and disappear with increasing order indicating they may be related to be modeling errors, e.g. the $T^m$ terms in the constant power region. Generally the largest co-efficient in the matrix is the most stable with increasing value of the degree, particularly if it is not on the boundary of the degree limit.

Apart from variation of the error in modelling with the degree of the equations, 4th degree equations were also chosen as this was the largest degree of the terms predicted by the analytical modeling in Section II.C. While the use of higher degree terms may produce improved fits, these[a1] are also more sensitive to small errors in the data being fitted.

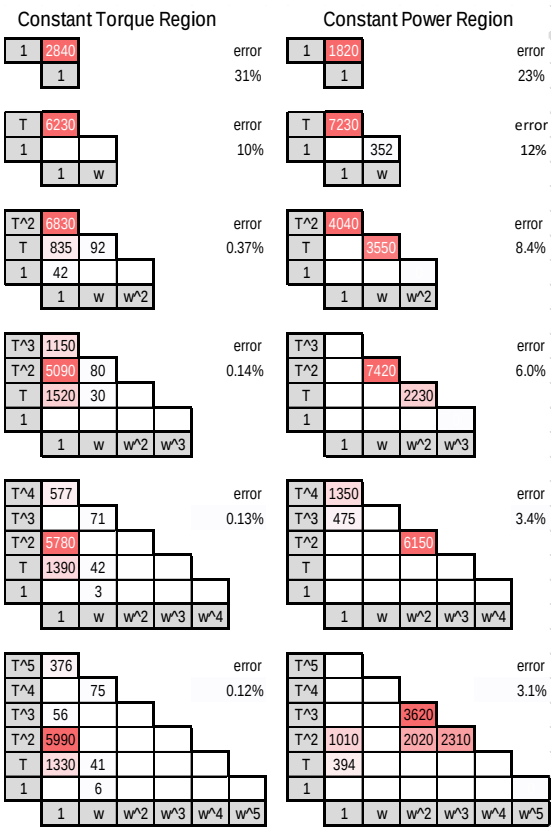


Figure 7. IPM stator copper loss. Constant torque and constant power region loss curve fits using zero to fifth-degree loss terms with non-negative co-efficients. Modeling errors are shown.

### B. *Effect of Allowing Negative Co-Efficients*

The above analysis assumes non-negative co-efficients. If this constraint is removed, three effects were found: firstly, the modeling error generally decreased; secondly, the positive co-efficients from Fig. 7 generally become larger and zero co-efficients become either negative or have a small positive value; and thirdly, while the constant torque co-efficients are not greatly affected when negative co-efficients are allowed, the constant power results show considerable "instability" with very large both positive and negative terms appearing (e.g. about –40kW for the $T^2$ co-efficient).

Allowing negative co-efficients makes it harder to interpret the loss breakdown. The negative loss terms are not practically meaningful in the context of the analytical results in Section II.C. Thus, forcing the co-efficients to positive values ensures consideration of only physical loss terms and makes the results less sensitive to small errors in the data.

### C. *Effect of Not Separately Curve-Fitting the Constant Torque and Power Regions*

The previous analysis has modeled the constant torque and constant power operating regions with separate curve fits. This subsection examines modeling the IPM stator copper loss over the entire torque-speed plane with a single curve.

Using a single function results in poorer modeling of the loss curves, particularly in the transition region between the constant torque and constant power regions. The constant torque co-efficients are reasonably accurately modeled. For the constant power region, the magnitude of the dominant $T^2\omega^2$ term is considerably smaller and a new $\omega^3$ term appears.

These results show that modelling the constant torque and power regions separately give a better fit to the calculated loss data and easier interpretation of the losses.

## V. Discussion of Curve-Fit Results

The first row of Fig. 4 shows the calculated efficency maps for the three machines. The IM has a peak efficiency of over 94% which is reached at medium to high speeds and medium output power. The IPM has a slightly higher peak efficiency (96%). It has a more triangular-shaped peak efficiency region corresponding to medium speeds and output powers. The SPM has a similar peak efficiency to the IPM but the high speed-dependent losses results in a smaller tear-drop-shaped maximum efficiency region. This occurs at low to medium speeds and medium output powers.

Figs. 4 and 5 showed the loss contours and their curve fits for the IM, IPM and SPM machines for each of the loss types. In Fig. 4, for each loss type, contour plots of the calculated and the curve-fitted results using the loss co-efficients is shown.

Fig. 5 shows the corresponding tables of loss co-efficients using a 4th degree fit with non-negative co-efficients for both the constant torque and constant power regions based on the results in Section IV. Rows 1 to 5 show matrices of the peak loss contribution in watts of each of the loss co-efficients for the five individual loss types. Row 6 shows the sum of the individual loss co-efficients for each machine. Row 7 shows the loss co-efficients obtained by curve fitting the total loss contour plot which shows similar but not identical results to the sixth row. Rows 8 and 9 are sums of the copper and non-copper loss co-efficients from the first five rows with the totals expressed as percentages to allow the relative contribution of each loss co-efficient to be more easily identified.

### A. *Copper Losses*

The copper losses are the dominant losses in all three machines. This can be seen as they have the largest peak loss co-efficients in watts in rows 1 to 5 of Fig. 5.

To help understand these results, Fig. 8 shows the stator current and copper loss versus torque characteristics at standstill. These correspond to the *y*-axis of the total loss plots in Fig. 4 as copper loss is the only loss which exists at zero speed. It shows that below 120 Nm, the SPM has the lowest copper loss and at higher torques the IPM has the lowest copper loss. The IM generally has the highest copper loss versus torque curve.

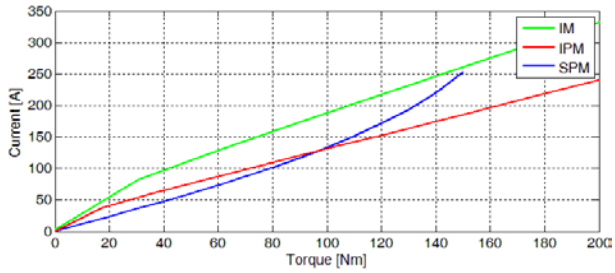


(a) Stator current vs torque

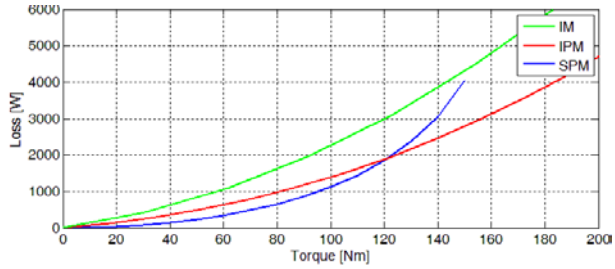


(b) Stator (and rotor) copper loss vs torque.

Figure 8. Calculated stator current and copper loss and versus torque at standstill [10]

These results are related to the constant torque data in Figs. 4 and 5. The constant torque co-efficients for the stator and rotor copper loss for the IM and the stator copper loss for the IPM in Fig. 5 have a similar distribution, see rows 1 and 3. From the relative sum of the copper loss co-efficients, see row 8, roughly 70-75% of the total IM and IPM copper loss occurs with the $T^2$ term and roughly 20-30% with the $T$ term. These results match the predictions in Section II that the $T$ and $T^2$ terms should be dominant based on a $T \propto I^2$ relationship at low currents and $T \propto I$ relationship at higher currents as seen in Fig. 8(a). While the number of data points is not sufficient at low currents to clearly see the shape of the torque vs current, it is clear that this is non-linear.

For the SPM, the current versus torque characteristic shows an initial linear relationship up to about 80Nm but then the current rapidly increases with torque producing the dominant $T^4$ loss component. Section II indicated that this is associated with $T \propto \sqrt{I}$ which implies heavy saturation.

The relative copper loss results in row 8 of Fig. 5 will now be examined.

All three machines in the constant torque region have only a small dependance between the stator copper loss and speed. The data in row 8 shows the speed dependent terms correspond to only about 2% of the total loss for all the machines.

In the constant power region, the IM and IPM machines have a dominant $T^2\omega^2$ stator copper loss component which implies a stator current proportional to output power ($T\omega$). As discussed in Section II this corresponds to a relatively low value of magnetising/*d*-axis current.

The SPM in the constant power region, has a similar dominant $T^4$ copper loss component as in its constant torque region. Like the IM and IPM, it has a strong $T^2\omega^2$ copper loss. Additionally it has a significant $\omega^2$ component due to the large flux-weakening *d*-axis current component which is mainly related to operating speed.

The dominant copper loss terms define the shape of the efficiency map. For instance for the IPM, the dominant loss term is $T^2$ in the constant torque region and $T^2\omega^2$ in the constant power region (see Fig. 5, row 1). By referring to the corresponding efficiency maps associated with these terms in Fig. 2(b), it can be seen that these[a2] shape the IPM efficiency map in Fig. 4, row 1.

### *B. Iron and Magnet Losses*

Fig. 9 shows the FE calculated no-load loss versus speed. It represents the *x*-axis of the total loss contour plot in Fig. 4. The no-load loss characteristic includes iron, magnet and no-load (flux-weakening) copper losses. It should be noted that the FE calculated results do not include any estimated mechanical losses such as bearing or windage.

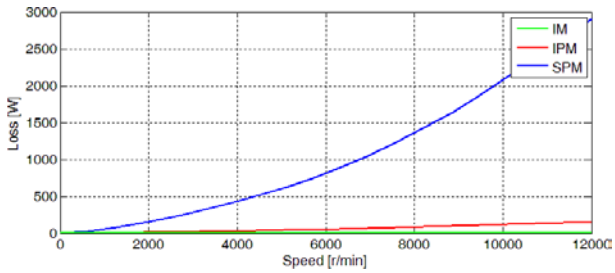


Figure 9. Calculated loss vs speed at no-load (excluding mechanical losses) [10]

The SPM has the highest no-load loss, which at maximum speed is comparable to its copper loss at its continuous torque capability. This is due to a combination of its high magnet loss and the large stator current required for field-weakening of the large back-emf voltage (over three times rated voltage) at this speed. The IPM no-load loss at maximum speed is small (150 W) due to its relatively low back-emf voltage which does not exceed rated voltage even at this speed. The IM has even lower electromagnetic losses under this condition.

Row 9 of Fig. 5 shows the combined iron and magnet losses for the three machines in both the constant torque and constant power regions. The majority of these losses occur in the terms: $\omega$, $\omega^2$, $\omega^3$, $T\omega$, $T\omega^2$ and $T\omega^3$. These loss terms are distinct from those associated with the copper losses (see row 8).

Row 2 of Fig. 5 shows the IM stator iron losses have a dominant $T\omega^2$ dependence in the constant torque region but this changes to $T\omega$ in the constant power region, likely due to the flux density reduction in this region. The peak iron losses are at medium to high torques in the constant power region (see Fig. 4).

For the IPM machine, rows 2, 4 and 5 of Fig. 5 show the stator iron losses are the largest of the non-copper losses, followed by the rotor iron losses. The magnet losses are negligible. In the constant torque region, the $T\omega$ term is the largest for the stator and rotor iron losses. In the constant power region, the dominant term is $T\omega^2$ term for the stator

iron losses but $T\omega^3$ for the rotor iron losses. These terms are likely related to harmonic iron losses produced by armature reaction. The highest iron losses occur at high loads at high speeds.

For the SPM machine, rows 2, 4 and 5 of Fig. 5 show the stator iron loss has a pronounced speed dependence and is much less dependent on torque, resulting in a dominant $\omega$ loss term in the constant torque and constant power regions. The $\omega$ rather than $\omega^2$ dependence is likely associated with a reduction in flux with speed. The rotor iron loss has a similar distribution to the IPM machine. The magnet losses are substantial in the SPM machine and are largest at high loads at high speeds. In the constant torque region the dominant term is $T\omega^2$, and in the constant power region the dominant terms is $\omega^3$.

## VI. Application Discussion

The loss modeling technique described in this paper can be applied to the analysis of calculated and experimental efficiency maps of electrical machines in four ways.

Firstly, a clear understanding of the mapping between the key types of losses, their resultant loss terms (e.g. $T^2\omega^2$) and the shape of the resultant efficiency map helps electric machine designers understand how to optimise their designs to meet particular application requirements. This also provides insights into the performance of different types of machines and aids in the selection of the most appropriate one for a specific application. For instance, high efficiency at high speeds is important for traction applications.

Secondly, for a calculated efficiency map, the loss co-efficients shown in rows 1 to 5 of Fig. 5 provide a convenient means for summarizing the key loss terms in the machine and their relative importance. This provides insights not only in which is the largest loss type of the machine, but also their variation with torque and speed in both constant torque and power regions.

Thirdly, the method provides a useful means to compare measured and FE calculated efficiency maps by allowing the identification of the likely loss components associated with any discrepancies. This uses a similar approach shown in in Table I except extended to the $k_{mn}T^m\omega^n$ loss terms. It requires the availability of detailed FE calculated individual loss component contour maps as shown in Fig. 4. The process involves comparing the loss term co-efficients of the total FE calculated loss map (Fig. 5, row 7) with those from the experimental loss map. The discrepancies in the co-efficients are then compared with the individual loss terms (Fig. 5, rows 1 to 5) to see which loss terms are most likely associated with the observed difference. Means to improve the modeling of these terms can then be investigated to obtain more accurate calculated results.

Fourthly, even without the FE calculated loss component maps, it is possible to use the information in rows 7 and 8 of Fig. 5 to approximately separate the experimental loss co-efficients into copper and non-copper loss terms in both constant torque and constant power regions. For instance, the rather crude separation proposed in Fig. 10, distinguishes the co-efficients relating to copper loss from other loss mechanisms. To test the accuracy of this approach, using this separation, the results in Table IV were obtained from the total loss modeling in row 7 of Fig. 5. These show a good correspondence between the estimated loss obtained by summing all the loss co-efficients within the region shown in Fig. 11 with the actual peak loss value calculated by finite-element analysis (in brackets). The error expressed as a fraction of the total FE loss for each machine has a maximum value of 17% and an average of 4%.

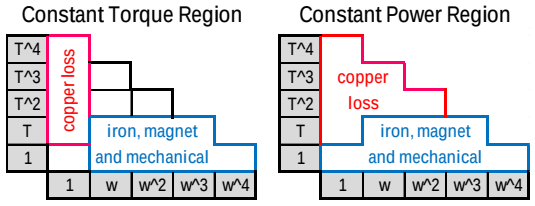


Figure 10. Approximate loss breakdown regions

TABLE IV. Prediction of Losses: Estimated from Selected Loss Co-efficients and FE calculated value in brackets

| | IM | IPM | SPM |
|---|---|---|---|
| **1. Constant Torque** | | | |
| a) copper losses (kW) | 7.81 (8.04) | 7.68 (7.87) | 3.85 (4.10) |
| b) iron and magnet (kW) | 1.33 (1.01) | 0.43 (0.36) | 0.60 (0.71) |
| | | | |
| **2. Constant Power** | | | |
| a) copper losses (kW) | 10.77 (13.21) | 7.83 (7.87) | 4.05 (4.10) |
| b) iron and magnet (kW) | 2.80 (1.40) | 1.81 (1.92) | 3.19 (3.78) |

## VII. Conclusions

This paper has examined the modeling and interpretation of efficiency maps for electric machines. It was based on a novel approach of using sum of the terms in the form of $k_{mn}T^m\omega^n$ to represent the variation of the stator and rotor copper, iron, magnet and the total losses with torque and speed. Analysis was used to predict the likely terms for each machine type. The proposed approach was tested using finite-element calculated efficiency maps of example induction, interior permanent magnet and surface permanent magnet machines. The following are the key results:

- the effect of each $T^m\omega^n$ loss co-efficient on the shape of the efficiency map was shown, and conversely, based on the shape of the efficiency map it was possible to roughly estimate the key loss co-efficients,
- accurate curve fitting of the loss contours was obtained by: using separate fits for both constant torque and constant power regions, ensuring the co-efficients were non-negative and using fourth-degree polynomials,
- while the largest loss co-efficients were readily found, care is necessary when interpreting coefficients with smaller magnitude as they can be significantly affected by the degree of the polynomial chosen,
- the key loss co-efficients found by fitting each of the FE calculated stator and rotor loss types were validated against the analytical predictions and checked against the static current-torque characteristics and no-load loss versus speed results,

- the normalised loss terms for each machine type were presented, and based on this a simple method to separate the loss co-efficients of copper loss and non-copper losses in both constant torque and constant power regions was proposed and validated.

The proposed method is a promising approach which allows machine designers to have more insight into the linkage between the stator and rotor loss types and the resultant efficiency map. It also potentially provides an improved means for comparing FE calculated with experimentally measured efficiency maps to identify the loss types responsible for any discrepancies. This aspect will be investigated in a future paper.

## REFERENCES


[1] S. S. Williamson, S. M. Lukic, and A. Emadi, "Comprehensive drive train efficiency analysis of hybrid electric and fuel cell vehicles based on motor-controller efficiency modeling," Power Electronics, IEEE Transactions on, vol. 21, pp. 730-740, 2006.

[2] J. O. Estima and A. J. M. Cardoso, "Efficiency Analysis of Drive Train Topologies Applied to Electric/Hybrid Vehicles," *IEEE Transactions on Vehicular Technology*, vol. 61, pp. 1021-1031, 2012.

[3] Tesla Motors, available: https://www.tesla.com/ [accessed: 14 Nov. 2016]

[4] L. Alberti, N. Bianchi, and S. Bolognani, "Variable-speed induction machine performance computed using finite-element," IEEE Trans. Ind. Appl., vol. 47, no. 2, pp. 789–797, Mar./Apr. 2011.

[5] D. F. Gosden, B. J. Chalmers, and L. Musaba, "Drive system design for an electric vehicle based on alternative motor types," in *Power Electronics and Variable-Speed Drives, 1994. Fifth International Conference on*, 1994, pp. 710-715.

[6] J. Goss, P. H. Mellor, R. Wrobel, D. A. Staton, and M. Popescu, "The design of AC permanent magnet motors for electric vehicles: A computationally efficient model of the operational envelope," in *Power Electronics, Machines and Drives (PEMD 2012), 6th IET International Conference on*, 2012, pp. 1-6.

[7] M. Ferrari, N. Bianchi, A. Doria, and E. Fornasiero, "Design of synchronous reluctance motor for hybrid electric vehicles," in *Electric Machines & Drives Conference (IEMDC), 2013 IEEE International*, 2013, pp. 1058-1065.

[8] K. Kiyota, H. Sugimoto, and A. Chiba, "Comparing Electric Motors: An Analysis Using Four Standard Driving Schedules," IEEE Industry Applications Magazine, vol. 20, pp. 12-20, 2014.

[9] X. Liu, D. Wu, Z. Q. Zhu, A. Pride, R. P. Deodhar and T. Sasaki, "Efficiency Improvement of Switched Flux PM Memory Machine over Interior PM Machine for EV/HEV Applications," IEEE Trans. Magns, vol. 50, no. 11, pp. 1-4, Nov. 2014.

[10] A. Mahmoudi, W. L. Soong, G. Pellegrino and E. Armando, "Efficiency maps of electrical machines," 2015 IEEE Energy Conversion Congress and Exposition (ECCE), Montreal, QC, 2015, pp. 2791-2799.

[11] G. Heins, D. M. Ionel, D. Patterson, S. Stretz, and M. Thiele, "Combined Experimental and Numerical Method for Loss Separation in Permanent-Magnet Brushless Machines," IEEE Transactions on Industry Applications, vol. 52, pp. 1405-1412, 2016.

[12] A. Mahmoudi, W. L. Soong, G. Pellegrino, and E. Armando, "Efficiency maps of electrical machines," in Energy Conversion Congress and Exposition (ECCE), 2015 IEEE, 2015, pp. 2791-2799.

[13] C.-Z. Liaw, D. M. Whaley, W. L. Soong, and N. Ertugrul, "Investigation of inverterless control of interior permanent-magnet alternators," Industry Applications, IEEE Transactions on, vol. 42, pp. 536-544, 2006.

[14] G. Pellegrino, A. Vagati, P. Guglielmi, and B. Boazzo, "Performance Comparison Between Surface-Mounted and Interior PM Motor Drives for Electric Vehicle Application," Industrial Electronics, IEEE Transactions on, vol. 59, pp. 803-811, 2012.

[15] G. Pellegrino, A. Vagati, B. Boazzo, and P. Guglielmi, "Comparison of Induction and PM Synchronous Motor Drives for EV Application Including Design Examples," Industry Applications, IEEE Transactions on, vol. 48, pp. 2322-2332, 2012.

[16] Infolytica, "Core Loss and Efficiency Calculations", available: http://www.infolytica.com/ [accessed: 30 June 2015].

[17] G. Pellegrino, T.M. Jahns, N. Bianchi, W. Soong and F. Cupertino, "The Rediscovery of Synchronous Reluctance and Ferrite Permanent Magnet Motors: Tutorial Course Notes." Springer Press, 2016.

[18] P. Sergeant and A. Van den Bossche, "Segmentation of magnets to reduce losses in permanent-magnet synchronous machines," IEEE Trans. Magn., vol. 44, no. 11, pp. 4409–4412, Nov. 2008.

[19] Mathworks, "Matlab Curvefitting Toolbox", available: https://au.mathworks.com/products/curvefitting/ [accessed: 14 Nov. 2016]